Effect of TiO2 on the Viscosity and Structure of Mineral Wool Melt from Blast Furnace Slag

Xiangdong Xing
Xi'an University of Architecture & Technology
Zhuogang Pang
Xi'an University of Architecture & Technology
Yueli Du
Xi'an University of Architecture & Technology
Jianlu Zheng
Xi'an University of Architecture & Technology
Shan Ren
Chongqing University
Jiantao Ju (2651198276@qq.com)
Xi'an University of Architecture & Technology

Research Article

Keywords: Mineral wool melt, Viscosity, Structure, Critical temperature, Activation energy

Posted Date: March 28th, 2020

DOI: https://doi.org/10.21203/rs.3.rs-19553/v1

Abstract

The effect of TiO2 on the viscous behaviours of mineral wool melts containing CaO–SiO2–Al2O3–MgO-TiO2 were studied at acidity coefficient Mk in the range of 1.0–1.6 and TiO2 content in the range of 0–6wt%. Based on the experimental data, the critical temperature and activation energy were calculated to analyse the changes in viscosity flow. The morphology and phase of slag were clarified by scanning electric microscopy with energy dispersive spectroscopy and X-Ray diffraction. Fourier transformation infrared and Raman spectra were used to obtain information about the variations in melt structure. The results showed that the viscosity decreased with increasing TiO2 content. The critical temperature (Tcr) was 1537–1645K, and it was relatively stable when the acidity coefficient Mk is 1.3. The activation energy decreased from 182.27, 178.48, 162.75 kJ/mol to 146.67, 139.28, 127.64 kJ/mol with increasing acidity coefficient Mk, respectively. With increasing TiO2 content, the fraction of main crystal phases (CaSiO3) decrease and form perovskite (CaTiO3). In addition, relationships are found to exist between the viscosity and structure of melt. The formation of Ti-O or O-Ti-O bonds weakens the stability of molten slag, and the number of bridging oxygen decreases from 1.85 to 0.65.

1. Introduction

Mineral wool is an excellent energy-saving insulation material widely used in various fields such as industrial, heat and sound insulation; energy conservation in buildings; and for decoration [1, 2]. Several methods are used to produce mineral fibres, including melt spinning method, rotating water spinning method, and melt extraction. Of these, melt spinning is most commonly used in mineral wool production, a process that consists of two primary steps: the melting of raw materials and centrifugal or blowing spinning. In this process, viscosity of mineral melt is one of the most important factors influencing processing operations and the quality of the mineral fibre [3, 4]. All of the production problems such as high shot content, large fibre diameter, short fibre length and volumetric melt flow deviation from the optimum processing condition are related to melt viscosity properties. In order to ensure efficient process operations, the viscosity of melt should be controlled within a suitable range [5], which is essential to maintain stable operation.

It is well known that viscosity is affected by both temperature and material composition, and the temperature during the production process is relatively stable, but the raw material composition is not identical. Of the raw materials of mineral wool (metallurgical slag, basalt, and others) [5, 6], blast furnace (BF) slag is widely used as its chemical composition (primarily composed of SiO_2, CaO, Al_2O_3 and MgO) is similar to the materials in mineral wool. However, a certain amount of TiO_2 is contained in blast furnace slag due to the addition of titanium ores and titanium-containing pellets during BF protection operations, which influences the viscosity of the mineral wool melts in the production process and further affects the quality of the mineral wool fibres. Therefore, it is critical to study the effect of TiO_2 on the viscosity of mineral wool melt.

Several studies have reported the effects of TiO_2 on the physicochemical properties of metallurgical slag. Yan et al. [7] reported that the viscosity of the quinary system CaO–SiO_2–8 wt%MgO–14 wt%Al_2O_3–TiO_2 with basicity (C/S = CaO/SiO_2) in the range of 0.5–1.3 and found TiO_2 decreased the viscosity of a quinary slag system. Saito et al. [8] revealed that the apparent activation energy of viscosity flow decreased and the structural units became smaller with increasing TiO_2 content in CaO-SiO_2-Al_2O_3 slag system. Gao et al. [9] proposed that the viscosity increased with the addition of TiO_2 in the range of 23.46 wt%–26.45 wt%, which is the result of the formation of high melting point perovskite. The viscosity experiments conducted by Park et al. [10] indicated that TiO_2 acted as a basic oxide and depolymerized complex silicate sheets into simpler structures in CaO-SiO_2-10 wt%MgO-17 wt%Al_2O_3 slag. Work by Jiao et al. [11] found TiO_2 lowered the viscosity of CaO-SiO_2-11.26 wt%Al_2O_3-9.13 wt%MgO-TiO_2-FeO slag and weaken the strength of the silicate network. Chang et al. [12] studied the effect of TiO_2 and MnO on the viscosities of CaO-SiO_2-MgO-Al_2O_3-TiO_2-MnO slag and discovered that the linkage between the [SiO_4] and [AlO_4] tetrahedra decreased with the addition of TiO_2. In conclusion, TiO_2 has been extensively investigated in metallurgical slag, but few studies have been conducted on the effect of TiO_2 on the viscous behaviour of mineral wool melt.

Therefore, in this study, the effect of TiO_2 on the viscosity of SiO_2-CaO-12 wt%Al_2O_3-8 wt%MgO slag containing TiO_2 content in the range of 0–6 wt% and an acidity coefficient (Mk) in the range of 1.0–1.6 was investigated by using a rotating cylinder viscometer. In addition, the critical temperature and activation energy were calculated to verify the structural changes of melts. And the morphology and crystallisation were examined using scanning electric microscopy with energy dispersive spectroscopy (SEM-EDS) and X-Ray diffraction (XRD). In addition, variations in the slag structure were qualitatively analysed using Fourier transformation infrared (FTIR) and Raman spectroscopy. The influence mechanism of TiO_2 on the viscosity and structure of mineral wool melt were clarified to provide a reference for the production of Ti-bearing mineral wool.

2. Experimental

2.1. Materials preparation

All experimental samples were prepared from analytical reagent grade powders of CaO, SiO2, Al2O3, MgO, and TiO_2. The materials used in the present work are listed in **Table 1.** These reagents were precisely weighed at 150g to form given compositions and then mixed completely in a Mo crucible. The crucible was then placed in an electric resistance furnace, heated to 1773K for pre-melting under Ar atmosphere (99.999%, 0.3 L/min) and maintained for 180 min to ensure a more uniform sample composition. The slag was then poured into water, and a number of pieces of the quenched sample were collected and divided into three portions. The first portion of the sample was used to measure the viscosity of the melt. The second part of sample was used to analyse the content of the chemical compositions of samples by X-Ray fluoroscopy (XRF, S4 Explorer; Bruker AXS, Germany). The results of XRF and the designed contents are included in Table 1. The last part of the quenched sample was used to analyse the slag structure

through FTIR (Nicolet 6700; Thermo Fisher Scientific, USA) and Raman (inVia Reflex; Renishawn, UK) spectroscopy. The Origin software was used to manipulate the FTIR curves, and Peakfit was used to subtract background and deconvolute the Raman spectra. Additionally, the quenched powders were verified to be amorphous by X-ray diffraction (XRD, D8 ADVANCE A25; Bruker AXS, Germany), which is presented in **Fig. 1**.

Table 1. Experimental compositions of slags (composition in wt %)

	Initial composition						Final composition by XRF analysis					
No.	CaO	SiO_2	Al_2O_3	MgO	TiO_2	Mk	CaO	SiO_2	Al_2O_3	MgO	TiO_2	Mk
1	42	38	12	8	0	1.0	41.89	37.98	11.97	8.06	0	1.00
2	41	37	12	8	2	1.0	40.92	37.01	12.08	7.93	2.06	1.00
3	40	36	12	8	4	1.0	40.08	35.95	11.87	7.96	3.92	1.00
4	39	35	12	8	6	1.0	38.90	35.13	11.95	8.05	5.97	1.00
5	35.48	44.52	12	8	0	1.3	35.47	44.62	12.03	7.88	0	1.31
6	34.60	43.40	12	8	2	1.3	34.63	43.36	12.06	7.97	1.98	1.30
7	33.74	42.26	12	8	4	1.3	33.69	42.37	11.95	7.97	4.02	1.30
8	32.87	41.13	12	8	6	1.3	32.83	41.17	11.93	8.04	6.03	1.30
9	30.46	49.54	12	8	0	1.6	30.50	49.51	12.01	7.96	0.02	1.60
10	29.69	48.31	12	8	2	1.6	29.71	48.27	11.98	8.03	2.01	1.60
11	28.92	47.08	12	8	4	1.6	29.03	46.97	12.06	7.98	3.96	1.59
12	28.15	45.85	12	8	6	1.6	28.12	45.90	11.97	8.01	6.00	1.60

2.2. Apparatus used for viscosity measurements

The slag viscosity measurement was conducted using the rotating cylinder method. The experimental apparatus is shown in detail in **Fig. 2**. The U-shaped MoSi2 heating element in the furnace was used to heat the apparatus. The furnace tube was composed of corundum and the experimental temperatures were controlled by a Pt-6%Rh and Pt-30%Rh thermocouple inserted into the furnace. The measurement error was less than ±2 K. When the rotating shaft was working, the torsion wire generated a twist angle due to the viscous action of the slag. The computer then converted the twist angle into a time difference signal and the slag viscosity values were calculated and recorded.

2.3. Experimental procedure

The viscosities of the slags were measured as follows. The pre-melted slag (110g) was held in a Mo crucible. The Mo crucible was placed in a constant temperature zone of the reaction chamber in the resistance furnace. The slag was heated to 1773K at the rate of 7K/min in Ar atmosphere and kept for 120 min to homogenize the composition of the slag before the spindle was immersed into the fluid slag. The viscosity measurements were performed during the cooling cycle with an equilibration time of 10 min at each temperature to ensure sufficient thermal equilibration. The measurements were also conducted above the critical temperature of the melt. The critical temperature for the $CaO–SiO_2–12wt\%Al_2O_3–8wt\%MgO–2.2wt\%\ TiO_2$ slag is shown in **Fig. 3**. When the temperature was lower than 1593K, the value

of the natural logarithm of the viscosity (lnη) increased significantly, indicating that the large solid phase began to precipitate, and the corresponding temperature was the critical temperature (T_{cr}). The viscometer was calibrated using castor oil of a known viscosity before each viscosity measurement. Following the viscosity measurements, the samples were heated to the critical temperature and kept for 90 min. The samples were then quenched on a water-cooled copper plate to confirm the morphology and element distribution using SEM-EDS (VEGA 3 XMU/XMH, Tescan, Czech Republic) and XRD, respectively.

3. Results And Discussion

3.1. Effect of TiO_2 on viscosity of slag

The viscosities of the mineral wool melts based on CaO-SiO_2-Al_2O_3-MgO-TiO_2 at varying temperatures with different acidity coefficients Mk are shown in **Fig. 4**. The viscosity of the melt decreased with the addition of TiO_2 at a fixed acidity coefficient Mk of 1.0, as shown in **Fig. 4(a)**. However, the viscosity increases with decreasing temperature and the reduced effect of TiO_2 on slag viscosity at a higher temperature. This was because the amount of excess thermal energy sufficiently modified the intricate network structure of the slag, and the effect of TiO_2 was relatively weaker than that of high temperature. The results were in good agreement with some previous studies. Sohn et al. [13] and Xu et al. [14] concluded that the complex network structure is depolymerised to simpler structure with the addition of TiO_2, which decreases the slag viscosity. On the other hand, TiO_2 connects with monomer ($[SiO_4]^{4-}$) to form Ti-O-Ti linkages that replace the Si-O-Si linkages, because the ionic radius of Ti^{4+} (0.61Å) is larger than that of Si^{4+} (0.41Å), the bond length of Ti-O (1.90Å) is longer than that of Si-O (1.60Å), the strength of Ti-O-Ti linkages are weaker than those of Si-O-Si and the complicated network structure becomes unstable. As a result, the viscosity decreases [15–17]. **Fig. 4(b)** shows that the increase in TiO_2 content lowers the viscosity of melt, which is consistent with the various trends in the acidity coefficient Mk at 1.0. The viscosity of slag with a greater acidity coefficient Mk is relatively high at the same temperature. Although the high temperature weakens the influence of TiO_2 on melt, the effect of TiO_2 on decreasing viscosity is still more obvious than for a lower acidity coefficient Mk. This indicates that the temperature of 1733 K is insufficient to modify the network structure completely. **Fig. 4(c)** shows clearly that the influences of TiO_2 and temperature on the viscosity of slag are basically constant. However, with a further increase in temperature to 1773K, the reductive effect of TiO_2 on the viscosity is still obvious. This may be because the mole fraction of complex silicate and aluminate unites increases with an increase in the acidity coefficient, and the slag structure tends to polymerise; however, the high temperature cannot completely destroy the network structure. TiO_2 still has a strong effect on the decrease in viscosity.

3.2. Effect of TiO_2 on critical temperature

The critical temperature (T_{cr}) is defined as the temperature at which the viscosity increases sharply or the slag behaves like non-Newtonian fluids in the cooling cycle [18–20]. The critical temperatures were obtained from the temperature corresponding to the point of contact of a line with a slope of -1 on the

viscosity curve. The effect of TiO_2 on the critical temperature of slag is shown in **Fig. 5**. With the action of TiO_2, the critical temperatures of the experimental slags were in the range of 1549–1645K, which indicates good melting properties and meets the requirements for mineral wool production. The decreasing amplitudes of T_{cr} were 41.42K, 31.09K, and 38.53K as the acidity coefficient Mk rose from 1.0 to 1.6. The critical temperature decreased with the increment of TiO_2 content in the range of 0–6 wt%, and the average decreasing range was 37.01K. This is assumed to be because TiO_2 acts as network modifier, depolymerising complex silicate tetrahedron to chain ($[Si_2O_7]^{6-}$) and monomer ($[SiO_4]^{4-}$). In addition, slag with high acidity coefficient has higher T_{cr}, and it is relatively stable when the acidity coefficient Mk is 1.3. Therefore, the effect of TiO_2 on the T_{cr} of melt is weak at an acidity coefficient Mk of 1.3, and TiO_2 has little effect on the process of mineral wool production.

3.3. Activation energy for viscous flow

All the viscosities of the slag were measured above the critical temperature. This means that all the molten slags were in the fluid region, and the melt behaved as Newtonian fluids. Thus, the Arrhenius-type equation was applied to express the temperature dependence of the viscosity η:

$$\eta = A \exp\left(\frac{E_\eta}{RT}\right) \quad (1)$$

Eq. (1) can be taken logarithmically and written as the following.

$$\ln\eta = \ln A + E_\eta\left(\frac{1}{RT}\right) \quad (2)$$

where η, A, E_η, R, and T are the viscosity, pre-exponential factor, apparent activation energy of the slag, gas constant (8.314J/mol·K), and absolute temperature, respectively.

The apparent activation energy represents the viscous flow barrier, which can be calculated from the relationship of 1/T and ln(η), and the variation reflects the change in slag structure. **Fig. 6** shows the natural logarithm of viscosity (lnη) as a function of the reciprocal temperature (1/T) for 0–6 wt% TiO_2 with an increase in the acidity coefficient Mk from 1.0 to 1.6. The fitting lines ($R^2 > 0.99$) are used to calculate the activation energy. The intercept and slope of the fitting line represent lnA and E_η/R, respectively. The apparent activation energy of melts is shown in **Fig. 7**.

The activation energy diminishes regularly with the addition of TiO_2 and the decrease in the acidity coefficient from 1.6 to 1.0. The value of E_η is higher than that of a low Mk with the same TiO_2 content. There can be two possible reasons for the decrease in activation energy. On the one hand, the formation of Ti-O or Si-O-Ti bonds weakens the stability of the slag structure. On the other hand, TiO_2 acts as basic oxide and simplifies the Si-O reticular complex structure to chain or monomer, and the degree of polymerisation (DOP) is reduced. The molar fraction of $[SiO_4]$-tetrahedral and $[AlO_4]$-tetrahedral units is

reduced with the decrease in the acidity coefficient Mk from 1.6 to 1.0, resulting in a diminished intricate network structure and a decreased activation energy.

3.4. Area scanning analysis and phase compositions

To understand the slag microstructure at the critical temperature, back-scattered electron images of quenched slags with acidity coefficients Mk of 1.3 were characterised with SEM-EDS, as shown in **Fig. 8.** The mineral wool melt clearly consists of both a solid phase and a liquid matrix. Large fractions of dendritic crystal, the main crystal, are marked '1' in the slag, and these disperse unevenly in the matrix. Combining with BSE image EDS analysis, the dendritic particles can be considered as $CaSiO_3$ (CS). In addition, the phases marked '2' represent the liquid matrix consisting of Ca, Si, Al, Mg, Ti, and O. The solid phase particles become finer and the crystal fraction decreases with the increase in TiO_2 content, suggesting that the resistance of slag flow decreases. Thus, the melt has lower viscosity at the same temperature with an increasing TiO_2 content. Moreover, some grey and black regions are marked '3', and their composition can be expressed roughly as $Ca_2Al_2SiTiO_9$ (Figs. 8(e)–(f)). With the increase in TiO_2 content from 2wt% to 6wt%, the Ti element gathers around the dendritic crystal. Finally, the Ti combines with Ca to form perovskite ($CaTiO_3$), which is marked '4', as shown in Fig. 8(h), and spinel, gehlenite, and diopside are present in the crystal (based on a rough analysis by EDS). In brief, the fraction of solid phases decreases with the increase in TiO_2 content. The main crystals are $CaSiO_3$, and Ti elements gather around CS to form $CaTiO_3$ when TiO_2 is added to slag.

The slags followed by furnace cooling are analysed via XRD. The patterns obtained are shown in **Fig. 9.** For the slag without any TiO_2, the crystalline phases such as anorthite ($Ca(Al_2Si_2)O_8$), calcium silicate ($CaSiO_3$), and spinel ($MgAl_2O_4$) exist and have high melting points to increase the resistance of the viscous flow. However, with increases in TiO_2 content, the characteristic gehlenite, calcium silicate, and spinel peaks become less pronounced, and the peak of spinel ($MgAl_2O_4$) disappears. In addition, a new peak of perovskite ($CaTiO_3$) appears, it may be caused by the reaction of TiO_2 and gehlenite, calcium silicate, and spinel, as seen in Figs. 8(e)–(h). Altogether, the addition of TiO_2 decreases the mass fraction of gehlenite, calcium silicate, and spinel while increasing that of perovskite.

3.4 Effect of TiO_2 on slag structure using FTIR spectroscopy

The structure of slag affects viscosity, and the formation of complex network structure leads to an increase in viscosity. **Fig. 10** represents the FTIR absorption spectra of all the quenched slags. According to previous studies [21–26], silicate slags are generally within the range of 1200 to 400 cm^{-1}. From **Fig. 10**, the spectra can be divided into three regions: 1200–760 cm^{-1}, 760–580 cm^{-1}, and near 500 cm^{-1}, which correspond to the symmetric stretching vibration of the $[SiO_4]$-tetrahedron, the asymmetric stretching vibration of the $[AlO_4]$-tetrahedron, and T-O-T (T: Si or Al) bending vibration, respectively. Furthermore, the vibration bands for the $[SiO_4]$-tetrahedron are assigned to , which represents the degree of polymerisation of slags and "n" is the number of bridging oxygen in the silicate tetrahedral structure

[27,28]. The , , and were detected at ~860cm^{-1} ([SiO_4]$^{4-}$, monomer), ~915cm^{-1} ([Si_2O_7]$^{6-}$, dimer), ~980cm^{-1} ([Si_3O_{10}]$^{8-}$, chain), and ~1060cm^{-1} ([Si_4O_{10}]$^{4-}$, sheet), respectively. The structural units and in the [AlO_4]-tetrahedron are shown in **Fig. 10**, and a legible peak appears near 670 cm^{-1}, which was caused by the [AlO_4]-tetrahedron.

Fig. 10(a) shows that there was a decreasing trend in the transmittance of [SiO_4]-tetrahedral vibration bands with increasing TiO_2 content. The reason for the decrement in the [SiO_4]-tetrahedron is that TiO_2 acts as network modifier, and it could form [TiO_4]-tetrahedral units and incorporate silicate structures to form Si-O-Ti units. It should be noted that the Ti-O bond is weaker than the Si-O bond. Thus, the transformation process weakens the stability of melt and decreases the viscosity of melt. Generally, TiO_2 is classified as amphoteric oxide [29,30], but it behaves like basic oxide when the slag is acidic and dissociates O^{2-} to destroy the network of [SiO_4]. The schematic in **Fig. 11** illustrates the effect on the structure of melt. The transmittance trough of the [AlO_4]-tetrahedron became shallow and the shoulder at 712cm^{-1} shifted to 708cm^{-1} with the addition of TiO_2, whereas the peaks near 670 cm^{-1} became less pronounced. This indicates that the distance of Al and O became shorter, the number of decreased, and the network structure was depolymerised. The peak of the T-O-T bending bond in the low wavenumber region gradually reduced from 314 a.u. to 112 a.u., which suggests that the T-O-T bending became less effective. Under an acidity coefficient Mk of 1.3, the broad band of the [SiO_4]-tetrahedron between 760cm^{-1} and 1200cm^{-1} was greatly decreased with the addition of TiO_2. Meanwhile, the / ratio dramatically decreased as a result of TiO_2, which represents the amount of bridge oxygen and DOP of slag reduce. Some distinct changes in the stretching vibration of the [AlO_4]-tetrahedron could be observed. In addition to the trough depth of the [AlO_4]-tetrahedron becoming inconspicuous, the trough width also decreased with an increase in TiO_2 content. Furthermore, it could be observed that the peak of T-O-T bending was gradually reduced from 253a.u. to 49a.u., which indicates a decrement in the linkage between the [SiO_4] or [AlO_4]-tetrahedron. The trends of the [SiO_4]-tetrahedron, [AlO_4]-tetrahedra and T-O-T bending at an acidity coefficient Mk of 1.6 were the same as in the previous results. However, the curves were not smooth compared with those of 1.0 and 1.3 with the same TiO_2 content. The results of FTIR spectra were consistent with the changes in viscosity.

3.5 Effect of TiO_2 on the slag structure using Raman spectroscopy

FTIR spectra are used in the qualitative analysis of slag structures, whereas a more definitive quantitative analysis is necessary to provide clear information on the variations in the changes of the structural units. Thus, in this study, Raman spectroscopy was used to quantifiably analyse the changes in these units.

Fig. 12 exhibits the Raman spectra of the quenched samples at an acidity coefficient Mk of 1.3. All the spectral curves are deconvoluted into a Gaussian function with a minimum correlation coefficient (R^2 > 0.99) based on Mysen et al. [31]. The spectral curve of slag is divided into a high frequency region (800–1200cm^{-1}) and low-frequency region (600–800cm^{-1}). The changes in peak intensity at different

frequencies represent the variations in bridging oxygen (BO) bond contents of m(Si, Al, Ti)-O-n(Si, Al, Ti) and the content of the Si-O-Si tetrahedra structural unit ( ). The characteristic peak of the original Raman spectra in the high-frequency region (800–1200cm^{-1}) shifts from 983cm^{-1} to 885cm^{-1} with the increasing TiO_2 content. This indicates that the simple silicate structure units gradually increase and that the DOP of melt is reduced.

In previous studies [28,31–34], the band in the region of 800–1200 cm^{-1} is deconvoluted into four typical peaks that label with the presence of tetrahedrally coordinated silicon (Q^0, Q^1, Q^2, Q^3) located at 850–880cm^{-1}, 900–920cm^{-1}, ~1000cm^{-1}, and ~1050cm^{-1}, respectively. In addition, the bands centred at 650–670cm^{-1} and near 725cm^{-1} appear in the low-frequency region, as shown in **Figs. 12(b) and (c)**. The corresponding Raman bands for the structural units are provided in **Table 2**.

Table 2. Corresponding Raman bands for the structural units

Frequencies (cm^{-1})	Assignments
~710	O-Ti-O or O-(Si, Ti)-O bonds
850–880	$[SiO_4]^{4-}$ (Q^0)
900–920	$[Si_2O_7]^{6-}$ (Q^1)
~1000	$[Si_2O_6]^{4-}$ (Q^2)
~1050	$[Si_2O_5]^{2-}$ (Q^3)

Fig. 12 and **Table 2** show obvious increasing trends of Q^0 and Q^1, whereas the fraction of Q^2 and Q^3 decreases with the increasing TiO_2 content. The peaks of the Ti-O and O-Ti-O bonds centred at near 650cm^{-1} and 710cm^{-1} appear when TiO_2 is added to slag, and that percentage increases with the addition of TiO_2. Reynard et al. [35] proposed that the Ti-O bonds in coordinated Ti^{4+} act as network modifiers at the frequency range of 600–650 cm^{-1}. Thus, the increment in the percentage of the Ti-O and O-Ti-O bonds suggests the intricate structure shifts to simpler structural units, and the viscosity decreases. The results of the spectra curves are not intuitive. Therefore, the specific data are given in subsequent discussions.

From the work of Frantz and Mysen [36], the relationship between the mole fractions of the structural units and the relative areas for the deconvoluted bands are expressed by the following relation:

$$X_i = \theta_i A_i \qquad (3)$$

where X_i is the mole fraction of species, θ_i is the Raman scattering coefficient, and A_i is the band area of the species.

However, because the Raman scattering coefficient is not an absolute value, which is derived from the absolute Raman intensity, calculating the relative abundances of different structural units from Raman spectra is difficult. Wu et al. [37] gave the four sensitivity factors S_i, which are the reciprocals of θ_i, where $S_0 = 1$, $S_1 = 0.514$, $S_2 = 0.242$, and $S_3 = 0.09$. Based on the results previously mentioned, the mole fractions of the structural units could be expressed by the following equation.

$$X_i = (A_i/S_i) / (\sum_{i=0}^{3} A_i/S_i) \quad (4)$$

where S_i is the reciprocal of θ_i.

The average number of bridging oxygen of slag on a Si atom (BO/Si) is obtained from the product sums of the mole fraction of the various structural unit species (X_i) and the corresponding bridging oxygen. The results of the average bridging oxygen number are summarised in **Table 3**.

Table 3. Results of the average bridging oxygen number in different slags

w(TiO_2)%	Q^0 (%)	Q^1 (%)	Q^2 (%)	Q^3 (%)	BO
0	7.67	18.84	54.05	19.44	1.85
2	10.36	29.71	35.54	24.39	1.74
4	30.21	18.18	33.61	16.00	1.39
6	51.74	34.28	11.31	2.67	0.65

It can be seen clearly that the content of Q^0 gradually increases, whereas Q^2 decreases with the increase in TiO_2 content. The fractions of Q^1 and Q^3 increase first with increasing of TiO_2 content from 0wt% to 2wt% and then decreases with the further addition of TiO_2 from 2wt% to 6wt%. This assumes that the Q^2 depolymerises to Q^1 or Q^3, which can be expressed by the following equation.

$$Q^2 \leftrightarrow Q^1 + Q^3 \quad (5)$$

It should be noted that the percentage of the complex network structure (Q^2 and Q^3) gradually decreases and the simple structure (Q^0 and Q^1) increases with TiO_2 content from 2wt% to 6wt%, which further proves that TiO_2 weakens the strength of the silicate structure and decreases the DOP of mineral wool melt.

4. Conclusion

The viscosity of mineral wool melt was measured under Ar atmosphere in fully liquid region, and the slag structure was verified using FTIR and Raman spectra. Good agreement was obtained among viscosity, critical temperature, activation energy, and changes in slag structure. The present study can be summarised as follows:

1. TiO_2 as a network modifier plays a role of depolymerisation in mineral wool melt, and the viscosity of slags decreases with increasing TiO_2 content from 0wt% to 6wt%.
2. The critical temperature and activation energy decrease with the addition of TiO_2 content, and the critical temperature is relatively stable when the acidity coefficient Mk is 1.3. Simultaneously, the

melting temperature is controlled between 1553K and 1773K, and the viscosity (0.513–2.214 Pa·s) meets the requirements of mineral wool production of mineral wool fibre.

3. TiO_2 reduces the fraction of solid phases ($CaSiO_3$). However, based on an observation of the slag crystallisation process with the addition of TiO_2, Ti combines with Ca to form perovskite ($CaTiO_3$).
4. The increase in TiO_2 causes an increase in Q^0 and Q^1 and a decrease in Q^2 and Q^3 in mineral wool melts. The amount of bridge oxygen gradually decreases, which lowers the DOP of slag.

Declarations

Acknowledgements

The present work was financially supported by the National Natural Science Foundation of China (Grant No.51604209) and Natural Science Basic Research Program of Shaanxi (Program No. 2019JLP-05). The authors gratefully acknowledge their support.

References

[1] Z.W. Chen, H. Wang, R. Ji, L.L. Liu, Christopher Cheeseman, X.D. Wang, Reuse of mineral wool waste and recycled glass in ceramic foams, ***Ceramics International.*** 45(2019) 15057-15064. DOI: 10.1016/j.ceramint.2019.04.242

[2] J. Yliniemi, O. Laitinen, P. Kinnunen, M. Illikainen, Pulverization of fibrous mineral wool waste, ***Journal of Material Cycles and Waste Management.*** 20(2018) 1248-1256. DOI: https://doi.org/10.1007/s10163-017-0692-3

[3] W.L. Wang, S.F. Dai, L.J. Zhou, J.K. Zhang, W.G. Tian, J.L. Xu, Viscosity and structure of MgO–SiO_2-based slag melt with varying B_2O_3 content, ***Ceramics International.*** 46(2020) 3631-3636. DOI: 10.1016/j.ceramint.2019.10.082

[4] J. Li, W.X. Liu, Y.Z. Zhang, A.M. Yang, K. Zhao, Research on modifying blast furnace slag as a raw material of slag fiber, ***Materials and Manufacturing Processes.*** 30(2015) 374-380. DOI: 10.1080/10426914.2014.973597

[5] D.W. Zhao, Z.T. Zhang, X.L. Tang, L.L. Liu, X.D. Wang, Preparation of slag wool by integrated waste-heat recovery and resource recycling of molten blast furnace slags: from fundamental to industrial application, ***Energies.*** 7(2014) 3121-3135. DOI: 10.3390/en7053121

[6] V.Fiore, T.Scalici, G.Di Bella, A.Valenza, A review on basalt fibre and its composites, ***Composites Part B-Engineering.*** 74 (2015) 74-94. DOI: 10.1016/j.compositesb.2014.12.034

[7] Z.M. Yan, X.W. Lv, W.C. He, J. Xu, Effect of TiO_2 on the liquid zone and apparent viscosity of SiO_2-CaO-8wt%MgO-14wt%Al_2O_3 system, ***ISIJ International.*** 57(2017) 31-36. DOI:

http://dx.doi.org/10.2355/isijinternational.ISIJINT-2016-420

[8] N. Saito, N. Hori, K. Nakashima, K. Mori, Viscosity of Blast Furnace Type Slags, ***Metallurgical and Materials Transactions B.*** 34(2003) 509-516. DOI: 10.1007/s11663-003-0018-9

[9] Y.H. Gao, L.T. Bian, Z.Y. Liang, Influence of B_2O_3 and TiO_2 on viscosity of titanium-bearing blast furnace slag, ***Steel Research International.*** 86 (2015) 386-390. DOI: 10.1002/srin.201400039

[10] H. Park, J.Y. Park, G.H. Kim, Il Sohn, Effect of TiO_2 on the viscosity and slag structure in blast furnace type slags, ***Steel Research International.*** 83(2012) 150-156. DOI: 10.1002/srin.201100249

[11] K.X. Jiao, J.L. Zhang, Z.Y. Chang, C.L. Chen, Y.X. Liu, Effect of TiO_2 and FeO on the Viscosity and structure of blast furnace primary slags, ***Steel Research International.*** 88(2017). DOI: https://doi.org/10.1002/srin.201600296

[12] Z.Y. Chang, K.X. Jiao, J.L. Zhang, X.J. Ning, Z.Q. Liu, Effect of TiO_2 and MnO on viscosity of blast furnace slag and thermodynamic analysis, ***ISIJ International.*** 58(2018) 2173-2179. DOI: https://doi.org/10.2355/isijinternational.ISIJINT-2018-379

[13] Il Sohn, W.L. Wang, H. Matsuura, F. Tsukihashi, D.J. Min, Influence of TiO_2 on the viscous behavior of calcium silicate melts containing 17 mass% Al_2O_3 and 10 mass% MgO, ***ISIJ International.*** 52(2012) 158-160. DOI: https://doi.org/10.2355/isijinternational.52.158

[14] R.Z. Xu, J.L. Zhang, R.Y. Ma, K.X. Jiao, Y.A. Zhao, Influence of TiO_2 on the viscosity of a high alumina slag and on carbon brick corrosion, ***Steel Research International.*** 89(2018), DOI: https://doi.org/10.1002/srin.201700353

[15] C.H. Jiang, K.J. Li, J.L. Zhang, Q.H. Qin, Z.J. Liu, M.M. Sun, Z.M. Wang, W. Liang, Effect of MgO/Al_2O_3 ratio on the structure and properties of blast furnace slags: A molecular dynamics simulation, ***Journal of Non-Crystalline Solids.*** 502(2018) 76-82. DOI: https://doi.org/10.1016/j.jnoncrysol.2018.06.043

[16] W.J. Huang, Y.H. Zhao, S. Yu, L.X. Zhang, Z.C. Ye, N. Wang, M. Chen, Viscosity property and structure analysis of $FeO–SiO_2–V_2O_3–TiO_2–Cr_2O_3$ slags, ***ISIJ International***. 56(2016) 594-601. DOI: http://dx.doi.org/10.2355/isijinternational.ISIJINT-2015-457

[17] R.B. Hadjean, V. Golabkan, J. P. Pereira-Ramos, A. Mantoux, D. Lincot, A Raman study of the lithium insertion process in vanadium pentoxide thin films deposited by atomic layer deposition, ***Journal of Raman Spectroscopy***. 33(2002) 631-638. DOI: 10.1002/jrs.893

[18] W.W. Xuan, J.S. Zhang, D.H. Xia, Crystallization Characteristics of a Coal Slag and Influence of Crystals on The Sharp Increase of Viscosity, ***Fuel.*** 176(2016), 102-109. DOI: http://dx.doi.org/10.1016/j.fuel.2016.02.062

[19] H. Kim, Il Sohn, Effect of CaF_2 and Li_2O Additives on the Viscosity of $CaO–SiO_2–Na_2O$ Slags, ***ISIJ International***. 51(2011) 1-8. DOI: https://doi.org/10.2355/isijinternational.51.1

[20] S. Sridhar, K.C. Mills, O.D.C. Afrange, H.P. Lörz, R. Carli. Break temperatures of mould fluxes and their relevance to continuous casting, ***Ironmaking & Steelmaking***. 27(2000) 283-242. DOI: 10.1179/030192300677534

[21] B.O. Mysen, F.J. Ryerson, D. Virgo, The Influence of TiO_2 on The Structure and Derivative Properties of Silicate Melts, ***American Mineralogist.*** 65(1980) 1150-1165.

[22] Y. Jiang, X.C. Lin, K. Ideta, H. Takebe, J. Miyawaki, S.H Yoon, I. Mochida, Microstructural transformations of two representative slags at high temperatures and effects on the viscosity, ***Journal of Industrial and Engineering Chemistry.*** 20(2014) 1338-1345. DOI: 10.1016/j.jiec.2013.07.015

[23] P.C. Li, X.J. Ning, Effects of MgO/Al_2O_3 Ratio and Basicity on the Viscosities of $CaO-MgO-SiO_2-Al_2O_3$ Slags: Experiments and Modeling, ***Metallurgical and Materials Transactions B.*** 47(2016) 446-457. DOI: https://doi.org/10.1007/s11663-015-0470-3

[24] S.M. Han, J.G. Park, Il Sohn, Surface kinetics of nitrogen dissolution and its correlation to the slag structure in the $CaO-SiO_2$, $CaO-Al_2O_3$, and $CaO-SiO_2-Al_2O_3$ slag system, ***Journal of Non-Crystalline Solids.*** 357(2011) 2868-2875. DOI: 10.1016/j.jnoncrysol.2011.03.023

[25] S.S. Jung, Il Sohn, Crystallization control for remediation of an Fe_tO-rich $CaO–SiO_2–Al_2O_3–MgO$ EAF waste slag, ***Environmental Science & Technology.*** 48(2014) 1886-1892. DOI: 10.1021/es404277w

[26] X.D. Xing, Z.G.Pang, C. Mo, S. Wang, J.T. Ju, Effect of MgO and BaO on viscosity and structure of blast furnace slag, ***Journal of Non-Crystalline Solids.*** 530(2020), https://doi.org/10.1016/j.jnoncrysol.2019.119801

[27] E.Z. Gao, W.L. Wang, L. Zhang, Effect of Alkaline Earth Metal Oxides on the Viscosity and Structure of the $CaO-Al_2O_3$-Based Mold Flux for Casting High-Al Steels, ***Journal of Non-Crystalline Solids.*** 473(2017) 79-86. DOI: http://dx.doi.org/10.1016/j.jnoncrysol.2017.07.029

[28] G. Padmaja, P. Kistaiah, Infrared and Raman spectroscopic studies on alkali borate glasses: evidence of mixed alkali effect, ***Journal of physical chemistry B.*** 113(2009) 2397-2404. DOI: 10.1021/jp809318e

[29] K. Hu, X.W. Lv, S.P. Li, W. Lv, B. Song, K.X. Han, Viscosity of $TiO_2-FeO-Ti_2O_3-SiO_2-MgO-CaO-Al_2O_3$ for High-Titania Slag Smelting Process, ***Metallurgical and Materials Transactions B.*** 49(2018) 1963-1973. DOI: https://doi.org/10.1007/s11663-018-1284-x

[30] X.D. Xing, J.L. Zhang, Z.Y. Wang, J.Q. Liang, Y.R. Liu, Enrichment research on direct reduction melting and separation TiO_2 of vanadium titano-magnetite slag by acid leaching, ***Light Metals.*** 11(2015) 45-49. DOI□10.13662/j.cnki.qjs.2015.11.011

[31] B.O. Mysen, D. Virgo, C.M. Scarfe. Relations between the anionic structure and viscosity of silicate melts-a Raman spectroscopic study, ***American Mineralogist.*** 65(1980) 690-710.

[32] Y.Q. Sun, Z.T. Zhang, L.L. Liu, X.D. Wang. FTIR, Raman and NMR investigation of CaO-SiO_2-P_2O_5 and CaO-SiO_2-TiO_2-P_2O_5 glasses, ***Journal of Non-Crystalline Solids.*** 420(2015) 26-33. DOI: 10.1016/j.jnoncrysol.2015.04.017

[33] L.B. Deng, X.F. Zhang, M.X. Zhang, X.L. Jia, Effect of CaF_2 on viscosity, structure and properties of CaO-Al_2O_3-MgO-SiO_2 slag glass ceramics, ***Journal of Non-Crystalline Solids.*** 500(2018) 310-316. DOI: https://doi.org/10.1016/j.jnoncrysol.2018.08.018

[34] P. McMillan, Structural studies of silicate glasses and melts-Applications and limitations of Raman spectroscopy, ***American Mineralogist.*** 69(1984) 622-644.

[35] B. Reynard, F. Guyot, High-temperature properties of geikielite ($MgTiO_3$-ilmenite) from high-temperature high-pressure Raman spectroscopy—some implications for $MgSiO_3$-ilmenite, ***Physics and Chemistry of Minerals.*** 21(1994) 441. DOI: 10.1007/BF00202274

[36] J.D. Frantz, B.O. Mysen, Raman spectra and structure of BaO-SiO_2, SrO-SiO_2 and CaO-SiO_2 melts to 1600°C, ***Chemical Geology.*** 121(1995) 155-176. DOI: 10.1016/0009-2541(94)00127-T

[37] Y.Q.Wu, G.C.Jiang, J.L.You, H.Y.Hou, H.Chen, Raman scattering coefficients of symmetrical stretching modes of microstructural units in sodium silicate melts, ***Acta Physica Sinica.*** 54(2005) 961-66. DOI: 10.7498/aps.54.961

[1] Z.W. Chen, H. Wang, R. Ji, L.L. Liu, Christopher Cheeseman, X.D. Wang, Reuse of mineral wool waste and recycled glass in ceramic foams, ***Ceramics International.*** 45(2019) 15057-15064. DOI: 10.1016/j.ceramint.2019.04.242

[2] J. Yliniemi, O. Laitinen, P. Kinnunen, M. Illikainen, Pulverization of fibrous mineral wool waste, ***Journal of Material Cycles and Waste Management.*** 20(2018) 1248-1256. DOI: https://doi.org/10.1007/s10163-017-0692-3

[3] W.L. Wang, S.F. Dai, L.J. Zhou, J.K. Zhang, W.G. Tian, J.L. Xu, Viscosity and structure of MgO–SiO_2-based slag melt with varying B_2O_3 content, ***Ceramics International.*** 46(2020) 3631-3636. DOI: 10.1016/j.ceramint.2019.10.082

[4] J. Li, W.X. Liu, Y.Z. Zhang, A.M. Yang, K. Zhao, Research on modifying blast furnace slag as a raw material of slag fiber, ***Materials and Manufacturing Processes.*** 30(2015) 374-380. DOI: 10.1080/10426914.2014.973597

[5] D.W. Zhao, Z.T. Zhang, X.L. Tang, L.L. Liu, X.D. Wang, Preparation of slag wool by integrated waste-heat recovery and resource recycling of molten blast furnace slags: from fundamental to industrial

application, ***Energies.*** 7(2014) 3121-3135. DOI: 10.3390/en7053121

[6] V.Fiore, T.Scalici, G.Di Bella, A.Valenza, A review on basalt fibre and its composites, ***Composites Part B-Engineering.*** 74 (2015) 74-94. DOI: 10.1016/j.compositesb.2014.12.034

[7] Z.M. Yan, X.W. Lv, W.C. He, J. Xu, Effect of TiO_2 on the liquid zone and apparent viscosity of SiO_2-CaO-8wt%MgO-14wt%Al_2O_3 system, ***ISIJ International.*** 57(2017) 31-36. DOI: http://dx.doi.org/10.2355/isijinternational.ISIJINT-2016-420

[8] N. Saito, N. Hori, K. Nakashima, K. Mori, Viscosity of Blast Furnace Type Slags, ***Metallurgical and Materials Transactions B.*** 34(2003) 509-516. DOI: 10.1007/s11663-003-0018-9

[9] Y.H. Gao, L.T. Bian, Z.Y. Liang, Influence of B_2O_3 and TiO_2 on viscosity of titanium-bearing blast furnace slag, ***Steel Research International.*** 86 (2015) 386-390. DOI: 10.1002/srin.201400039

[10] H. Park, J.Y. Park, G.H. Kim, Il Sohn, Effect of TiO_2 on the viscosity and slag structure in blast furnace type slags, ***Steel Research International.*** 83(2012) 150-156. DOI: 10.1002/srin.201100249

[11] K.X. Jiao, J.L. Zhang, Z.Y. Chang, C.L. Chen, Y.X. Liu, Effect of TiO_2 and FeO on the Viscosity and structure of blast furnace primary slags, ***Steel Research International.*** 88(2017). DOI: https://doi.org/10.1002/srin.201600296

[12] Z.Y. Chang, K.X. Jiao, J.L. Zhang, X.J. Ning, Z.Q. Liu, Effect of TiO_2 and MnO on viscosity of blast furnace slag and thermodynamic analysis, ***ISIJ International.*** 58(2018) 2173-2179. DOI: https://doi.org/10.2355/isijinternational.ISIJINT-2018-379

[13] Il Sohn, W.L. Wang, H. Matsuura, F. Tsukihashi, D.J. Min, Influence of TiO_2 on the viscous behavior of calcium silicate melts containing 17 mass% Al_2O_3 and 10 mass% MgO, ***ISIJ International.*** 52(2012) 158-160. DOI: https://doi.org/10.2355/isijinternational.52.158

[14] R.Z. Xu, J.L. Zhang, R.Y. Ma, K.X. Jiao, Y.A. Zhao, Influence of TiO_2 on the viscosity of a high alumina slag and on carbon brick corrosion, ***Steel Research International.*** 89(2018), DOI: https://doi.org/10.1002/srin.201700353

[15] C.H. Jiang, K.J. Li, J.L. Zhang, Q.H. Qin, Z.J. Liu, M.M. Sun, Z.M. Wang, W. Liang, Effect of MgO/Al_2O_3 ratio on the structure and properties of blast furnace slags: A molecular dynamics simulation, ***Journal of Non-Crystalline Solids.*** 502(2018) 76-82. DOI: https://doi.org/10.1016/j.jnoncrysol.2018.06.043

[16] W.J. Huang, Y.H. Zhao, S. Yu, L.X. Zhang, Z.C. Ye, N. Wang, M. Chen, Viscosity property and structure analysis of FeO–SiO_2–V_2O_3–TiO_2–Cr_2O_3 slags, ***ISIJ International***. 56(2016) 594-601. DOI: http://dx.doi.org/10.2355/isijinternational.ISIJINT-2015-457

[17] R.B. Hadjean, V. Golabkan, J. P. Pereira-Ramos, A. Mantoux, D. Lincot, A Raman study of the lithium insertion process in vanadium pentoxide thin films deposited by atomic layer deposition, ***Journal of Raman Spectroscopy***. 33(2002) 631-638. DOI: 10.1002/jrs.893

[18] W.W. Xuan, J.S. Zhang, D.H. Xia, Crystallization Characteristics of a Coal Slag and Influence of Crystals on The Sharp Increase of Viscosity, ***Fuel.*** 176(2016), 102-109. DOI: http://dx.doi.org/10.1016/j.fuel.2016.02.062

[19] H. Kim, Il Sohn, Effect of CaF_2 and Li_2O Additives on the Viscosity of $CaO–SiO_2–Na_2O$ Slags, ***ISIJ International***. 51(2011) 1-8. DOI: https://doi.org/10.2355/isijinternational.51.1

[20] S. Sridhar, K.C. Mills, O.D.C. Afrange, H.P. Lörz, R. Carli. Break temperatures of mould fluxes and their relevance to continuous casting, ***Ironmaking & Steelmaking***. 27(2000) 283-242. DOI: 10.1179/030192300677534

[21] B.O. Mysen, F.J. Ryerson, D. Virgo, The Influence of TiO_2 on The Structure and Derivative Properties of Silicate Melts, ***American Mineralogist.*** 65(1980) 1150-1165.

[22] Y. Jiang, X.C. Lin, K. Ideta, H. Takebe, J. Miyawaki, S.H Yoon, I. Mochida, Microstructural transformations of two representative slags at high temperatures and effects on the viscosity, ***Journal of Industrial and Engineering Chemistry.*** 20(2014) 1338-1345. DOI: 10.1016/j.jiec.2013.07.015

[23] P.C. Li, X.J. Ning, Effects of MgO/Al_2O_3 Ratio and Basicity on the Viscosities of $CaO-MgO-SiO_2-Al_2O_3$ Slags: Experiments and Modeling, ***Metallurgical and Materials Transactions B.*** 47(2016) 446-457. DOI: https://doi.org/10.1007/s11663-015-0470-3

[24] S.M. Han, J.G. Park, Il Sohn, Surface kinetics of nitrogen dissolution and its correlation to the slag structure in the $CaO-SiO_2$, $CaO-Al_2O_3$, and $CaO-SiO_2-Al_2O_3$ slag system, ***Journal of Non-Crystalline Solids.*** 357(2011) 2868-2875. DOI: 10.1016/j.jnoncrysol.2011.03.023

[25] S.S. Jung, Il Sohn, Crystallization control for remediation of an Fe_tO-rich $CaO–SiO_2–Al_2O_3–MgO$ EAF waste slag, ***Environmental Science & Technology.*** 48(2014) 1886-1892. DOI: 10.1021/es404277w

[26] X.D. Xing, Z.G.Pang, C. Mo, S. Wang, J.T. Ju, Effect of MgO and BaO on viscosity and structure of blast furnace slag, ***Journal of Non-Crystalline Solids.*** 530(2020), https://doi.org/10.1016/j.jnoncrysol.2019.119801

[27] E.Z. Gao, W.L. Wang, L. Zhang, Effect of Alkaline Earth Metal Oxides on the Viscosity and Structure of the $CaO-Al_2O_3$-Based Mold Flux for Casting High-Al Steels, ***Journal of Non-Crystalline Solids.*** 473(2017) 79-86. DOI: http://dx.doi.org/10.1016/j.jnoncrysol.2017.07.029

[28] G. Padmaja, P. Kistaiah, Infrared and Raman spectroscopic studies on alkali borate glasses: evidence of mixed alkali effect, ***Journal of physical chemistry B.*** 113(2009) 2397-2404. DOI: 10.1021/jp809318e

[29] K. Hu, X.W. Lv, S.P. Li, W. Lv, B. Song, K.X. Han, Viscosity of TiO_2-FeO-Ti_2O_3-SiO_2-MgO-CaO-Al_2O_3 for High-Titania Slag Smelting Process, ***Metallurgical and Materials Transactions B.*** 49(2018) 1963-1973. DOI: https://doi.org/10.1007/s11663-018-1284-x

[30] X.D. Xing, J.L. Zhang, Z.Y. Wang, J.Q. Liang, Y.R. Liu, Enrichment research on direct reduction melting and separation TiO_2 of vanadium titano-magnetite slag by acid leaching, ***Light Metals.*** 11(2015) 45-49. DOI□10.13662/j.cnki.qjs.2015.11.011

[31] B.O. Mysen, D. Virgo, C.M. Scarfe. Relations between the anionic structure and viscosity of silicate melts-a Raman spectroscopic study, ***American Mineralogist.*** 65(1980) 690-710.

[32] Y.Q. Sun, Z.T. Zhang, L.L. Liu, X.D. Wang. FTIR, Raman and NMR investigation of CaO-SiO_2-P_2O_5 and CaO-SiO_2-TiO_2-P_2O_5 glasses, ***Journal of Non-Crystalline Solids.*** 420(2015) 26-33. DOI: 10.1016/j.jnoncrysol.2015.04.017

[33] L.B. Deng, X.F. Zhang, M.X. Zhang, X.L. Jia, Effect of CaF_2 on viscosity, structure and properties of CaO-Al_2O_3-MgO-SiO_2 slag glass ceramics, ***Journal of Non-Crystalline Solids.*** 500(2018) 310-316. DOI: https://doi.org/10.1016/j.jnoncrysol.2018.08.018

[34] P. McMillan, Structural studies of silicate glasses and melts-Applications and limitations of Raman spectroscopy, ***American Mineralogist.*** 69(1984) 622-644.

[35] B. Reynard, F. Guyot, High-temperature properties of geikielite ($MgTiO_3$-ilmenite) from high-temperature high-pressure Raman spectroscopy—some implications for $MgSiO_3$-ilmenite, ***Physics and Chemistry of Minerals.*** 21(1994) 441. DOI: 10.1007/BF00202274

[36] J.D. Frantz, B.O. Mysen, Raman spectra and structure of BaO-SiO_2, SrO-SiO_2 and CaO-SiO_2 melts to 1600℃, ***Chemical Geology.*** 121(1995) 155-176. DOI: 10.1016/0009-2541(94)00127-T

[37] Y.Q.Wu, G.C.Jiang, J.L.You, H.Y.Hou, H.Chen, Raman scattering coefficients of symmetrical stretching modes of microstructural units in sodium silicate melts, ***Acta Physica Sinica.*** 54(2005) 961-66. DOI: 10.7498/aps.54.961

Figures

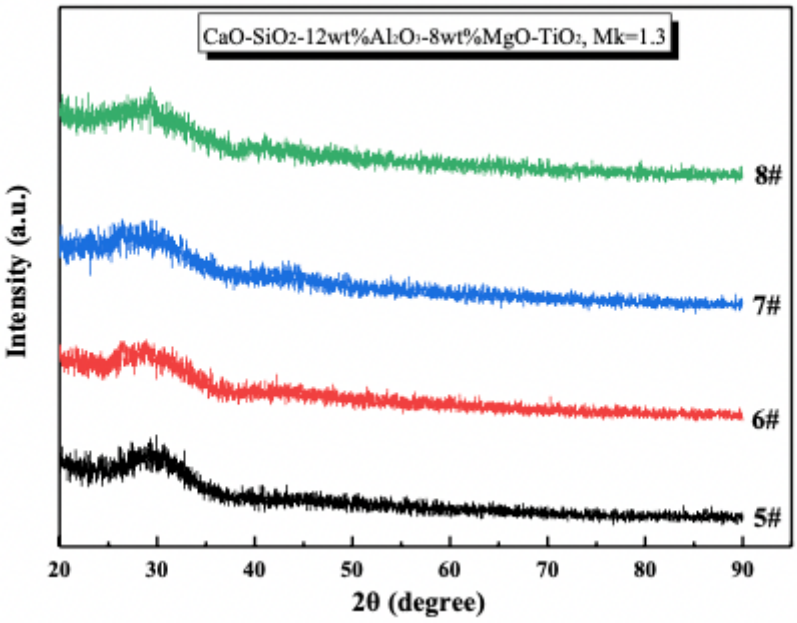

Figure 1

The XRD pattern of SiO2-Al2O3-CaO-MgO-TiO2 slag

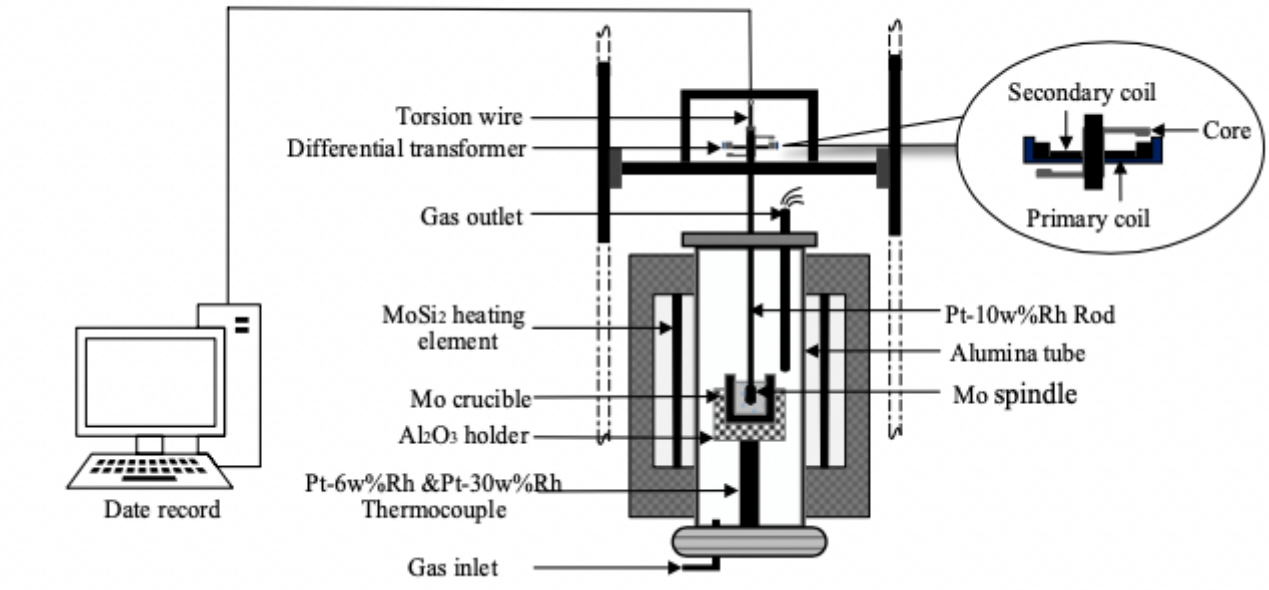

Figure 2

Schematic of the experimental apparatus

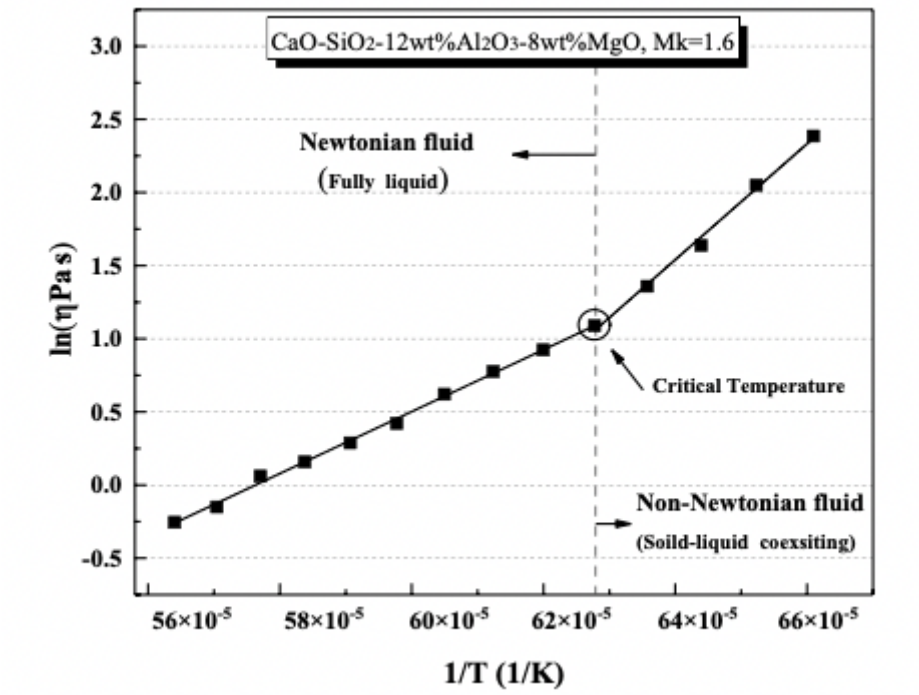

Figure 3

Critical temperature of CaO-SiO2-Al2O3-MgO at Mk = 1.6

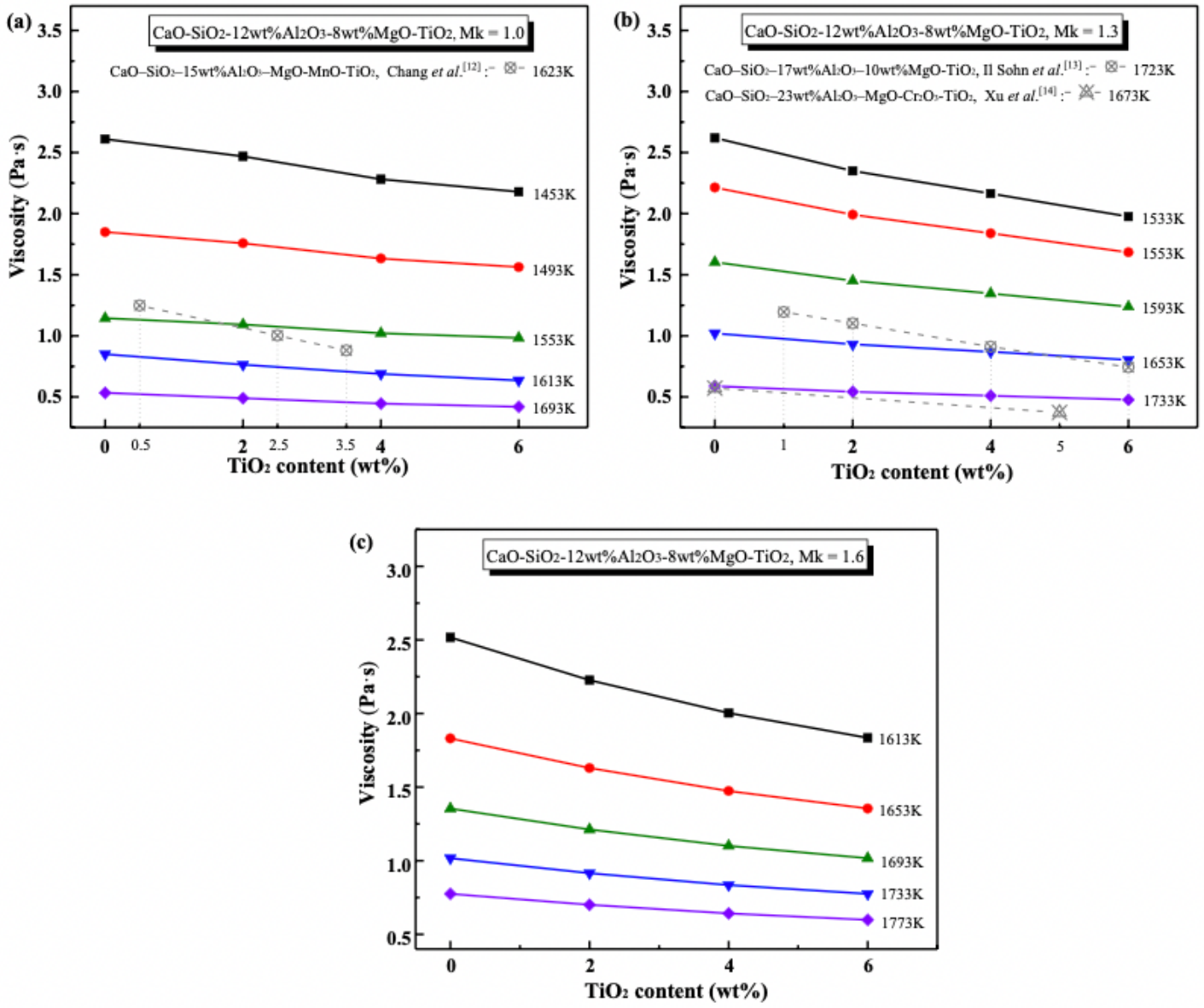

Figure 4

Effect of TiO2 on viscosity of the CaO-SiO2-Al2O3-MgO-TiO2-based slags at different temperatures and acidity coefficients: a) acidity coefficient Mk = 1.0; b) acidity coefficient Mk = 1.3; c) acidity coefficient Mk = 1.6

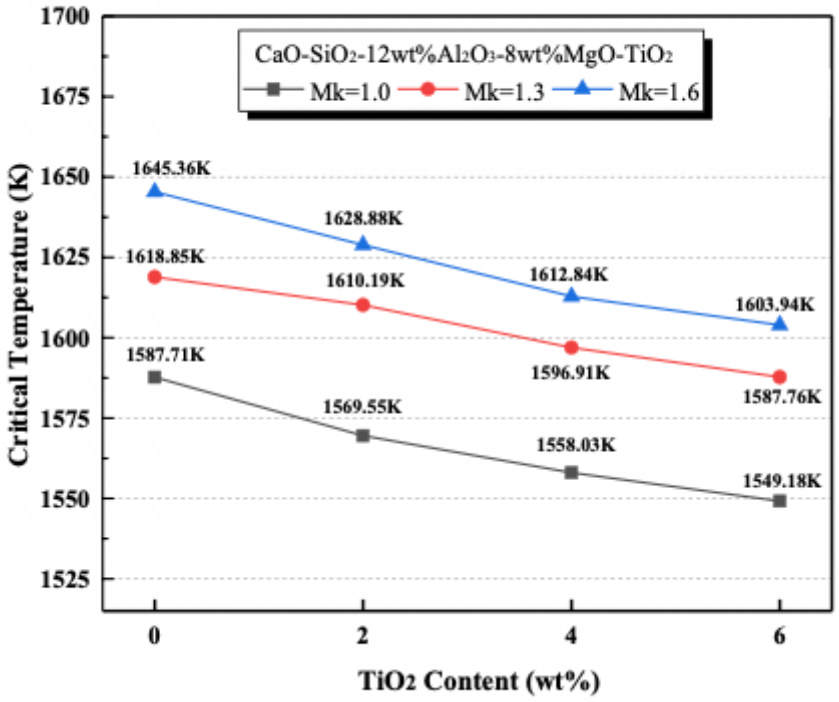

Figure 5

Effect of TiO2 on the critical temperature of slag

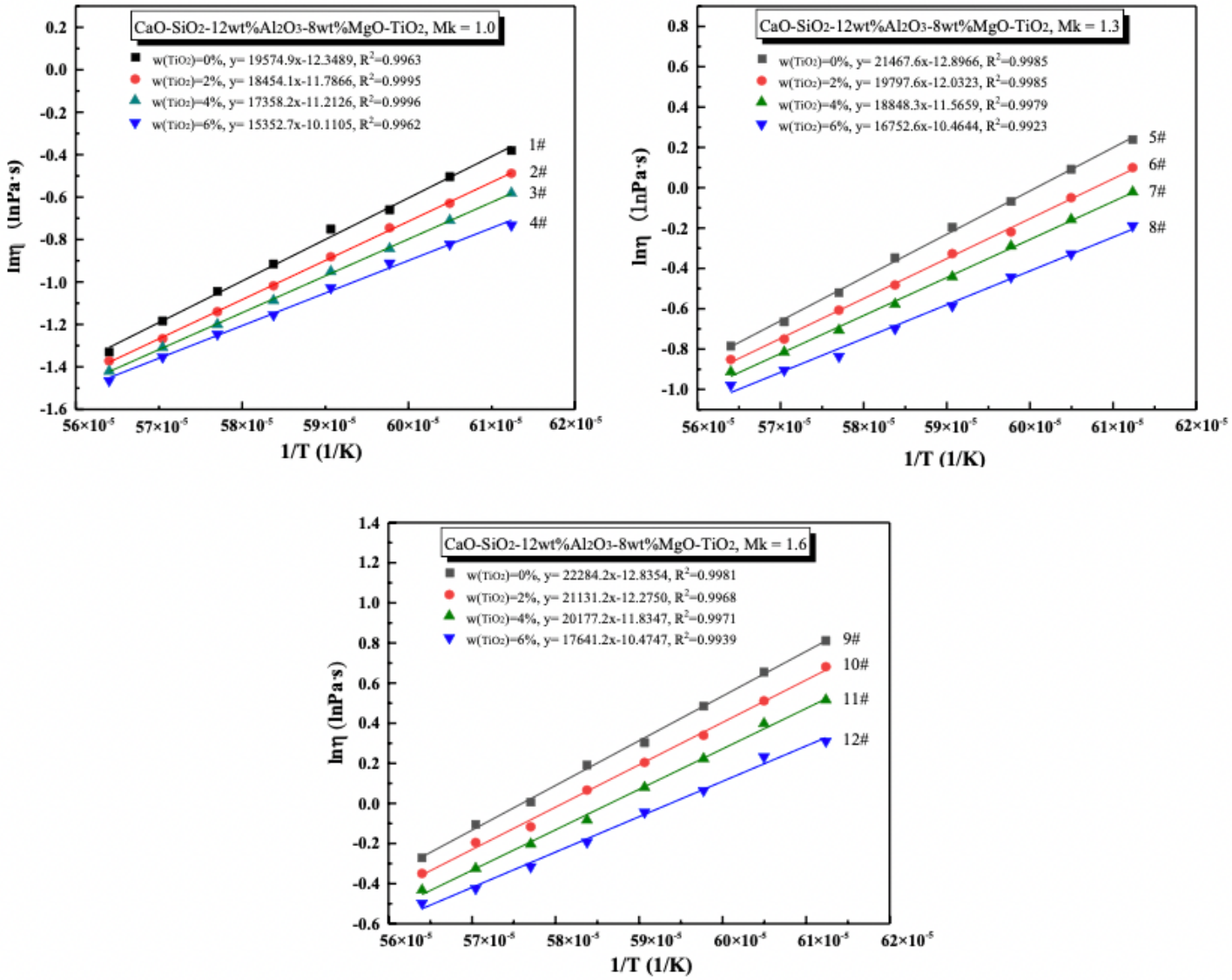

Figure 6

lnη versus 1/RT with all slags in the fully liquid region

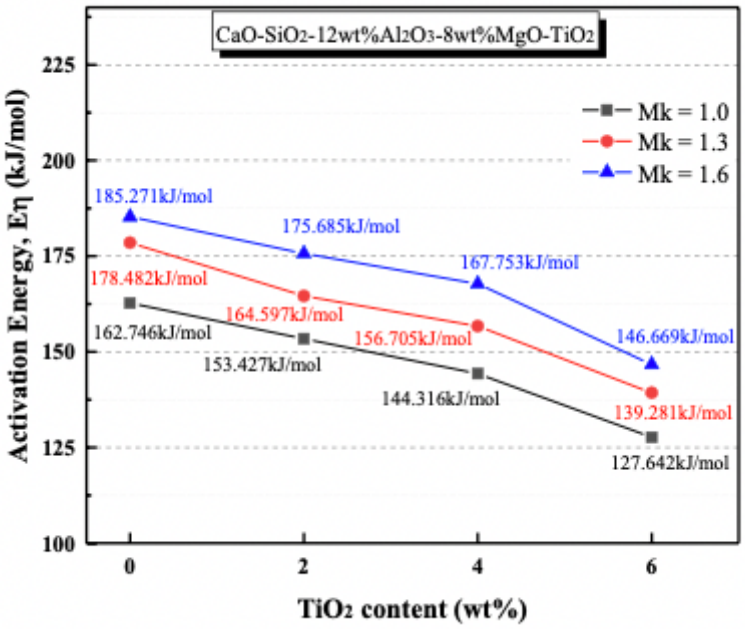

Figure 7

Apparent activation energy of melts

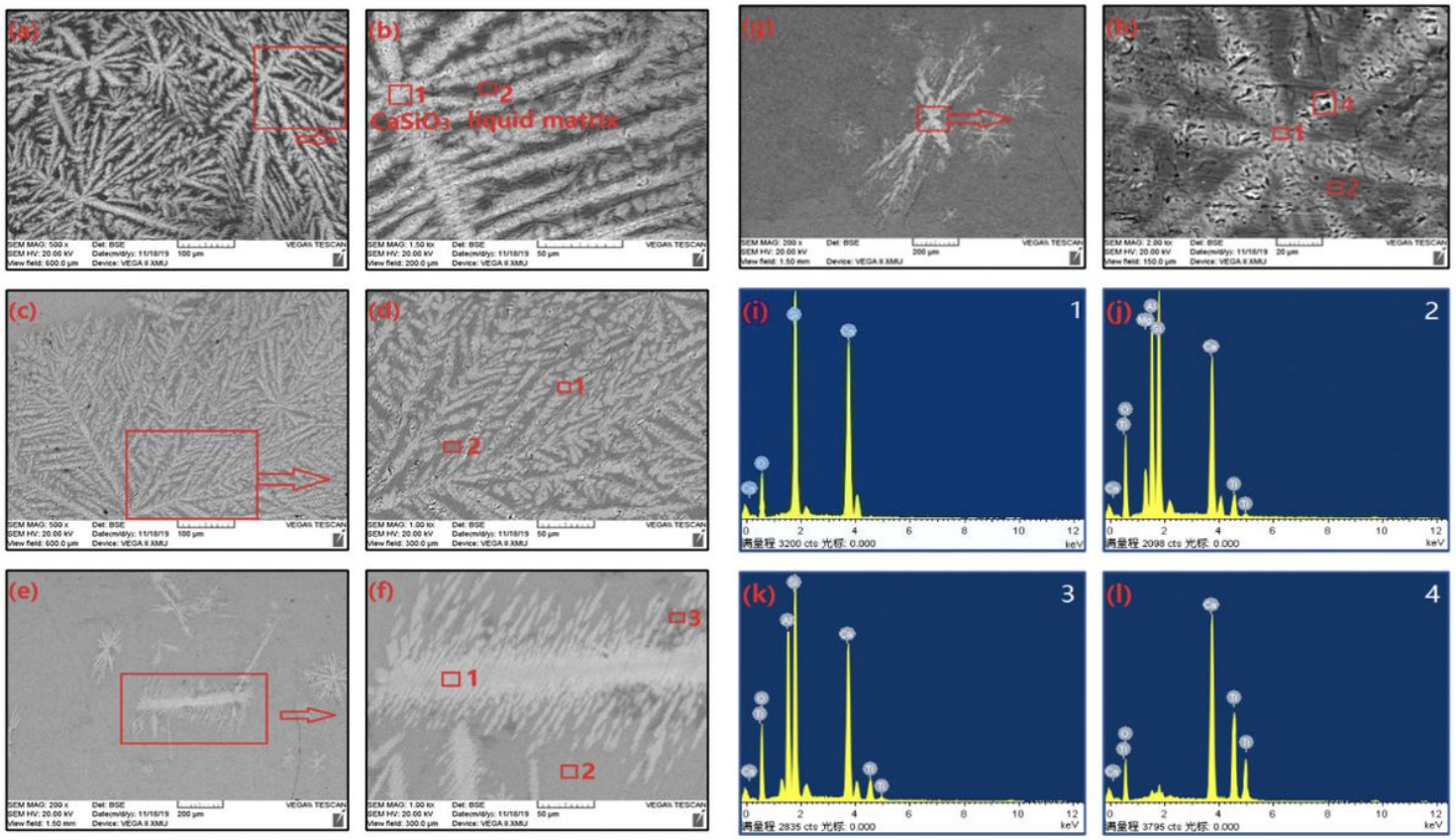

Figure 8

SEM images and EDS results of mineral wool melts with acidity coefficients Mk of 1.3 at the critical temperature. (a)-(h): BSE images of melts; (i)-(l): EDS results of phases marked “1” to “4”, where “1” indicates CaSiO3; “2” liquid phases; “3” MgAlTiO6; and “4” CaTiO3

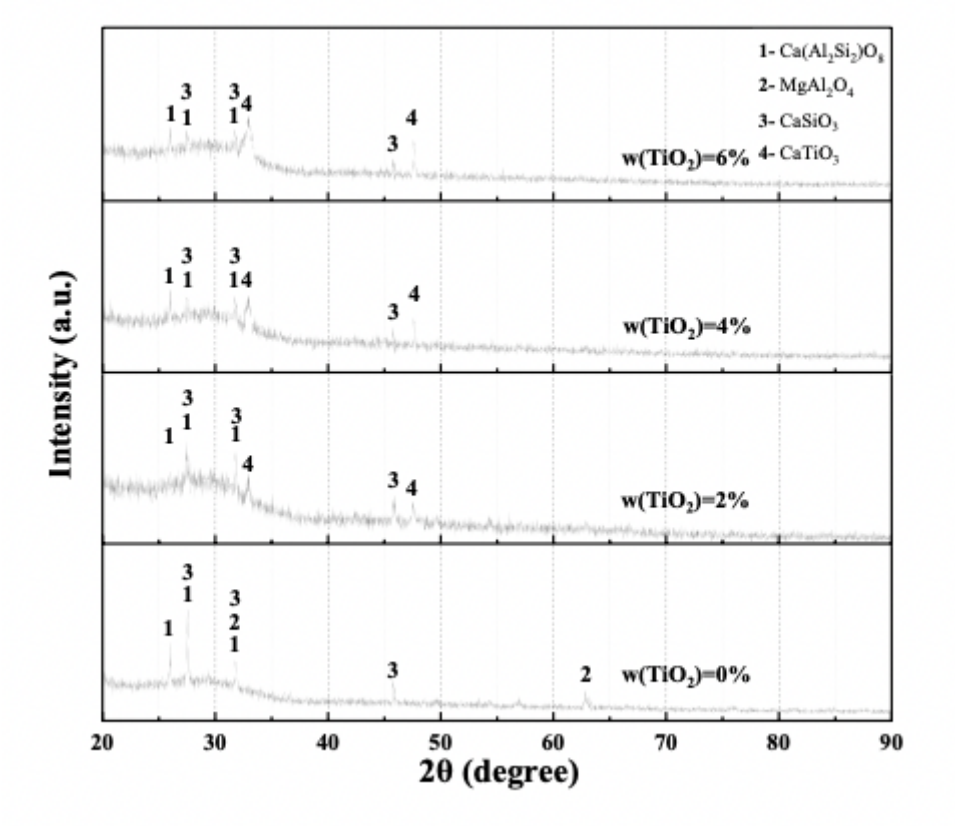

Figure 9

XRD patterns of mineral wool melt with different TiO2 content (Mk=1.3)

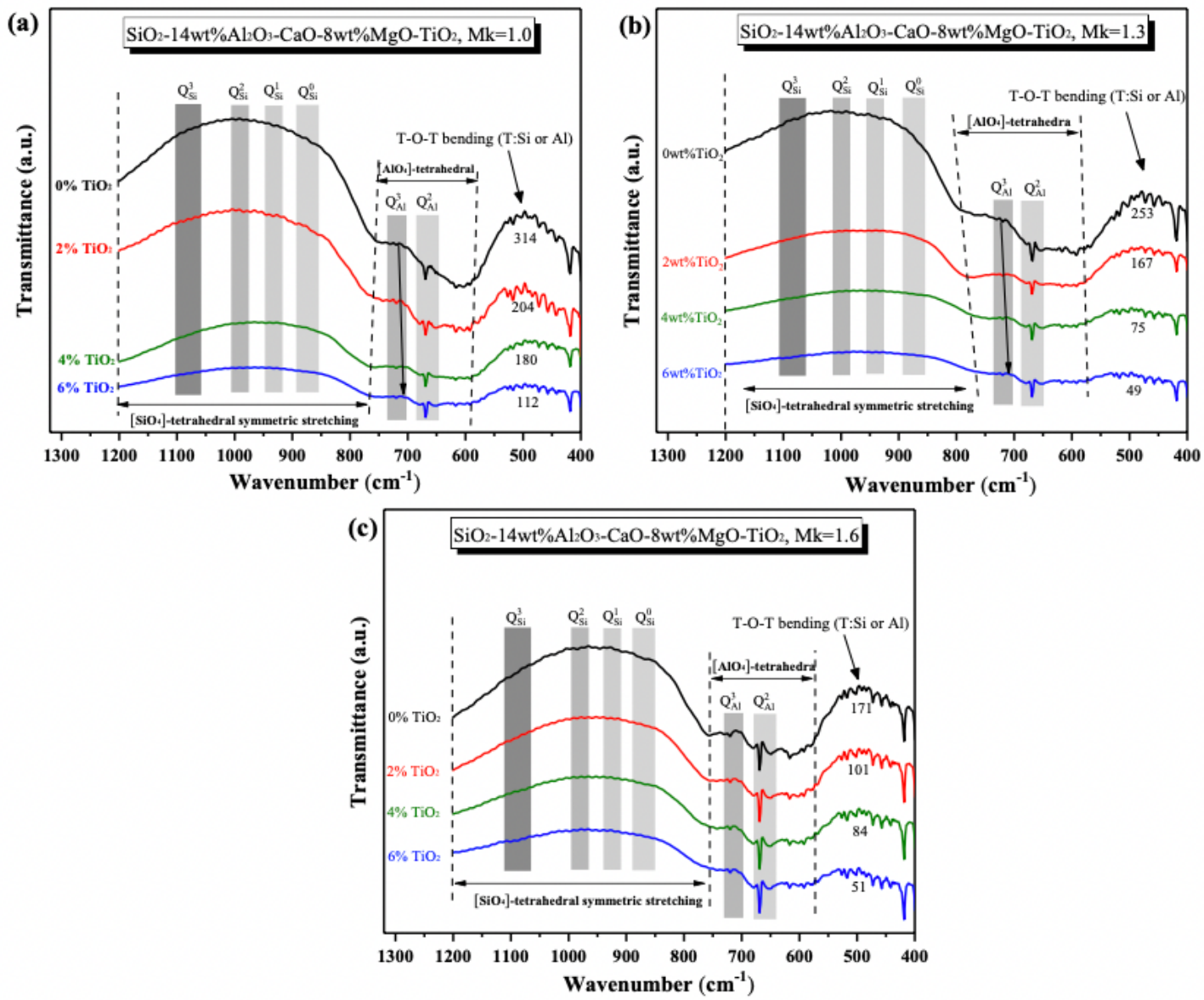

Figure 10

FTIR results of the as-quenched samples with various TiO2 content. a) acidity coefficient Mk = 1.0; b) acidity coefficient Mk = 1.3; c) acidity coefficient Mk = 1.6

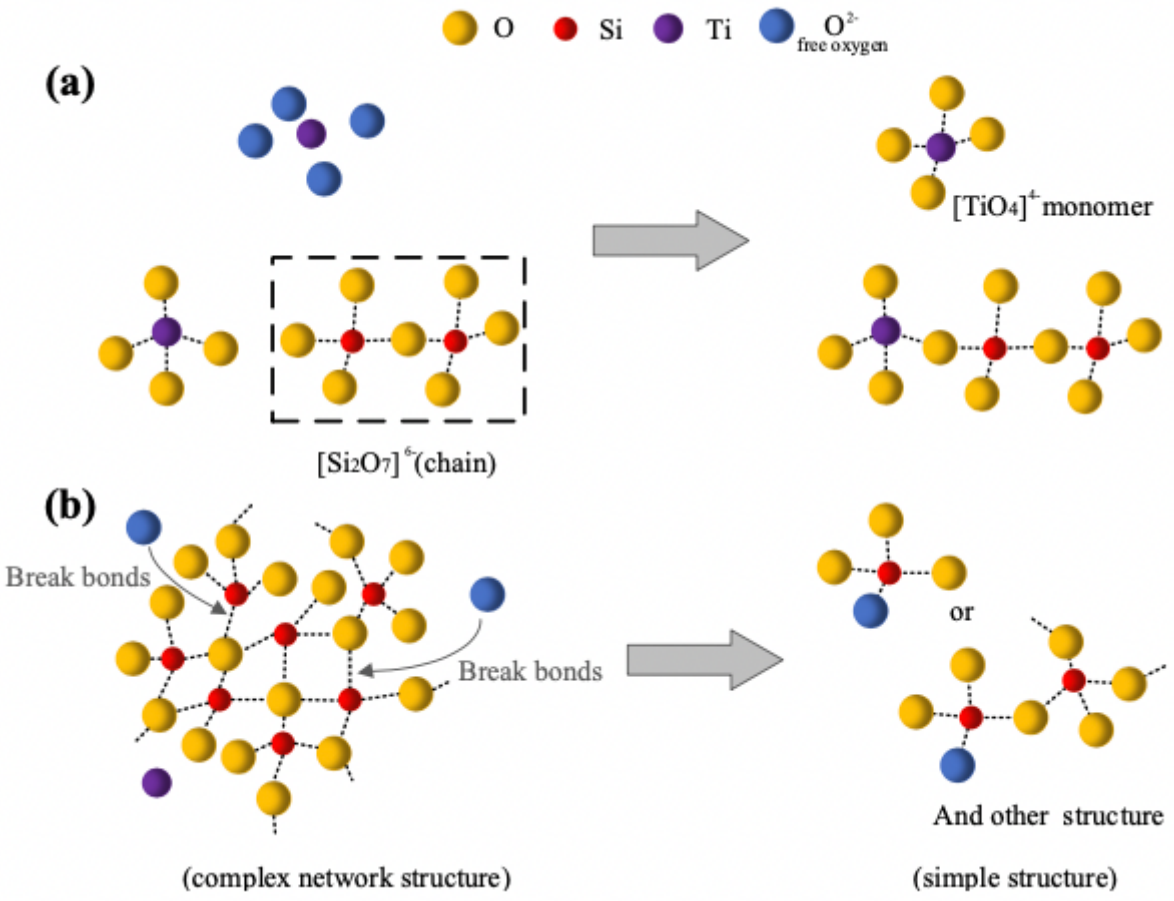

Figure 11

Schematic showing the effect on the structure of melt (a) transformation process of Ti4+ substitute for Si4+ in tetrahedral; (b) depolymerisation process of Si-O bonds

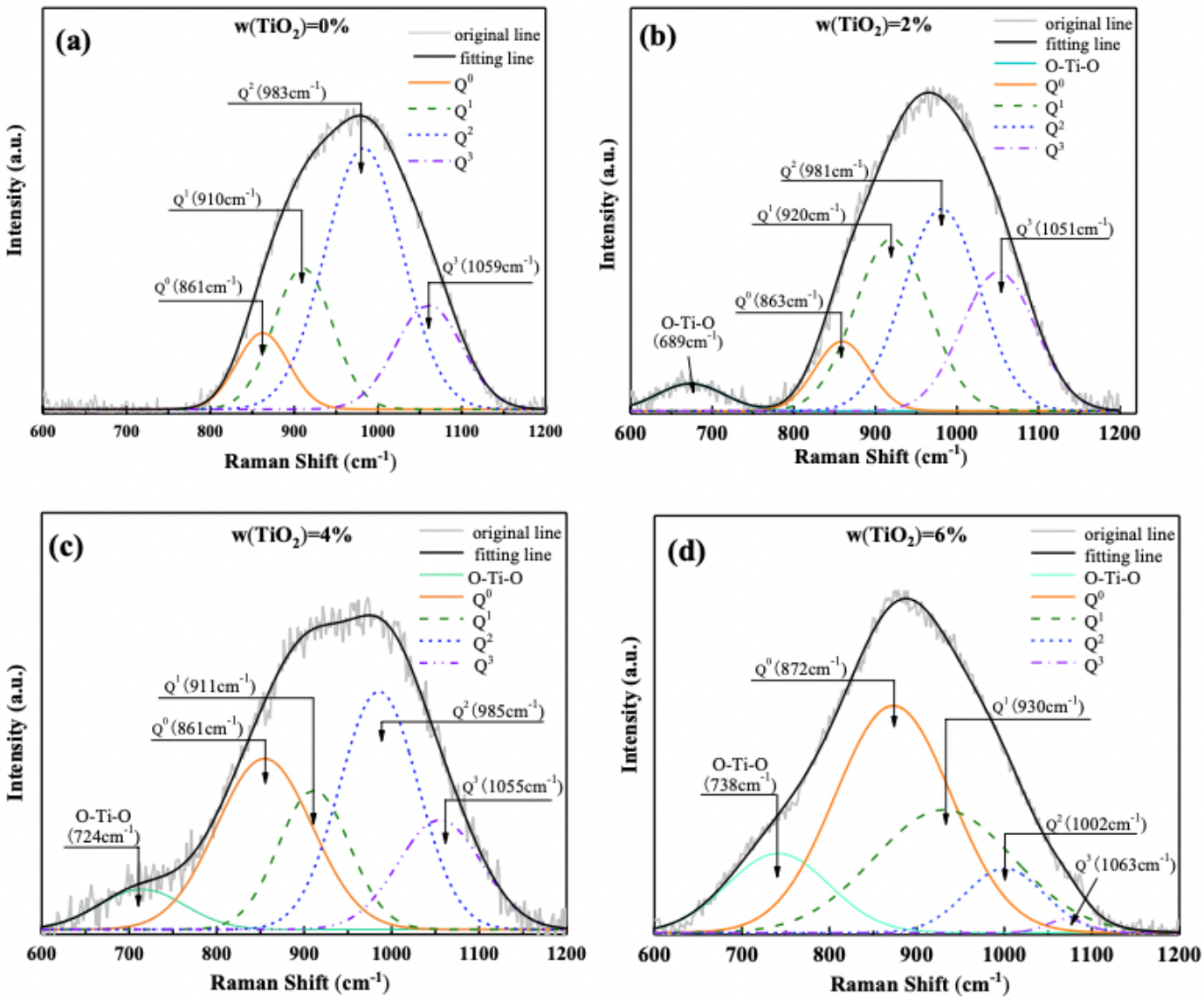

Figure 12

Raman spectra of quenched samples with different TiO2 content: a) 0wt% TiO2; b) 2wt% TiO2; c) 4wt% TiO2; d) 6wt% TiO2